



An ultrafast and robust structural damage identification framework enabled by an optimized extreme learning machine

Xinwei Wang^a, Yinghao Zhao^{b,c}, Zhihao Wang^a, Nan Hu^{d,e,f,*}

^a School of Civil Engineering and Communication, North China University of Water Resources and Electric Power, Zhengzhou 450045, China

^b School of Civil and Engineering Management, Guangzhou Maritime University, Guangzhou 510725, China

^c Guangdong Provincial Key Laboratory of Green Construction and Intelligent Operation & Maintenance for Offshore Infrastructure, Guangzhou Maritime University, Guangzhou 510725, China

^d State Key Laboratory of Subtropical Building and Urban Science, Guangzhou 510640, China

^e School of Civil Engineering and Transportation, South China University of Technology, Guangzhou 510641, China

^f Pazhou Lab, Guangzhou 510335, China



ARTICLE INFO

Keywords:

Damage identification
Extreme learning machine
Chaos game optimization
Ensemble empirical mode decomposition

ABSTRACT

Artificial intelligence (AI) has recently been implemented in structural health monitoring (SHM) systems for damage detection and identification. However, existing AI methods often involve a high number of parameters, resulting in the laborious workload during model training and implementation. In this study, we develop a lightweight damage identification framework embedded with an optimized extreme learning machine (ELM) using a significantly reduced number of parameters from frequency features of the structural vibrational signals. Coupled with the ensemble empirical mode decomposition (EEMD), the frequency features were abstracted from the structural vibrational signals in the data pre-processing step. Then, a metaheuristic algorithm (chaos game optimization, CGO) was chosen to optimize the model weight of the ELM to guarantee damage identification accuracy. Once the model is trained, the structural damages can be precisely identified despite the noise-contaminated data. We validated the efficiency and accuracy of the proposed framework with a public database and compare its performance with several common metaheuristic algorithms. With the proven capability, the proposed framework shows a promising future as a handy and reliable AI-assisted digital tool for robust development in next-generation structural monitoring systems.

1. Introduction

The service life of buildings and large-scale infrastructures would be shortened due to severe material and structural damage caused by extreme loads and/or environmental conditions. To achieve a longer service period, detecting and identifying structural damage is a crucial task in the field of structural health monitoring (SHM) [1]. The most popular structural damage identification method usually relies on vibrational signals measured at locations where stakeholders may concern. Collected vibrational signals require less human involvement and are no-biased than traditional visual inspections [2,3]. Measured signals can be processed and analyzed via either parametric or non-parametric methods [4]. Parametric methods extract physical characteristics, such as modal properties, frequencies, and damping from the measured signals. These characteristics can be used to evaluate the impact of different damages on the structural

* Corresponding author at: State Key Laboratory of Subtropical Building and Urban Science, Guangzhou 510640, China.
E-mail address: nanh02@scut.edu.cn (N. Hu).

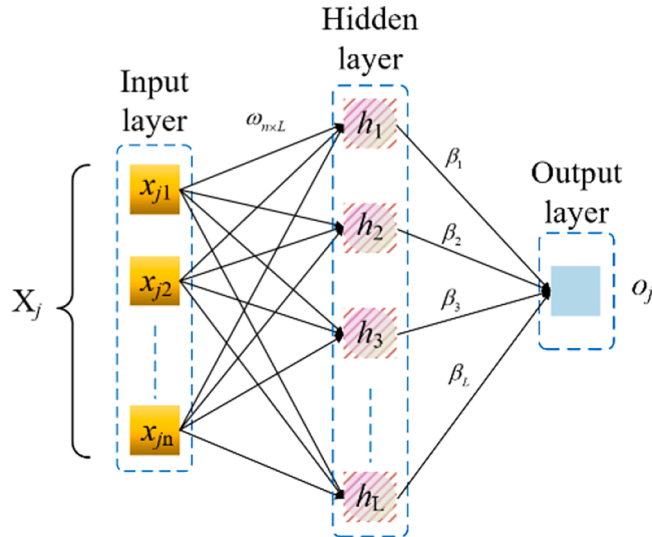


Fig. 1. The typical structure of the ELM.

dynamic response [1,5,6]. In contrast, the non-parametric methods employ mathematical or statistical approaches to identify structural damages based on the measured signals [7,8]. It is well recognized that using non-parametric methods is more robust than the parametric methods because various data-processing techniques could be used and a wide range of indicators or features can be extracted without knowing the actual structural physical characteristics [9,10].

Existing studies using non-parametric methods have attempted to introduce different machine learning (ML) techniques for property prediction and damage identification [11,12]. With appropriate inputs, a classifier can establish an accurate mapping relation between the actual signals and the structural damages. Mainstream efforts have implemented deep neural networks (DNNs) to process and classify data, such as Swin transformer [13], deep forest, and convolutional neural networks (CNNs). Despite these efforts, DNNs are sophisticated in general and could contain millions of weight parameters. For example, the widely-used Resnet [14] with the simplest version (i.e., Resnet-18) contains a total of 18 layers of neurons (i.e., more than ten million trainable parameters). This giant volume of parameters not only takes a longer training time but also requires a redundant testing time once the model is trained. An alternative route used shallow networks such as the traditional artificial neural networks (ANNs). Although a simple three-layer ANN only has about 10,000 trainable parameters, its accuracy is usually worse than those of DNNs. Challenges remain in reducing the complexity of the classifier and maintaining the accuracy of the damage identification.

To address the issues above, we introduced the extreme learning machine (ELM) model in this study [15], which is a network with a simple structure, faster training speed, and better predictive ability. Unlike CNNs or other DNNs, ELM is mathematically proven effective in supervised and unsupervised learning. Beyond neural networks alone, coupled models are also prevalent among ML to improve the regression and/or classification accuracy of NNs [11,16]. Several coupled models were recently proposed, such as the ant lion optimization (ALO)-NN [17], wind-driven optimization (WDO)-NN [18], and genetic algorithm (GA)-NN [19], in which their efficiency has been proved in various fields [20–22]. Thus, we implemented a coupled model (CGO-ELM) combining ELM with a novel metaheuristic algorithm the chaos game optimization (CGO) [23] for structural damage identification. The selection of CGO was based on its tremendous advantages in calculation speed and accuracy compared with existing optimization algorithms such as particle swarm optimization (PSO) and ant colony optimization (ACO) [23,24].

Prior to the damage identification using the CGO-ELM model, key signal features must be extracted using mathematical models [25–27] or data processing methods, such as the Hilbert-Huang transform [7,28], wavelet transforms [29] and S transform [30]. The quality of the inputs (i.e., abstract features from the original signals) is essential for the regression and/or classification accuracy of structural damage identification [31,32]. However, existing methods such as wavelet scalograms [33], 2D grayscale images [34], and sequential frequency data series [35] usually have a high-order dimension, leading to the increased complexity of the classifier. In this study, the ensemble empirical mode decomposition (EEMD) [36] is used to reduce the input data dimension and enhance the noise immunity of the proposed method. The intrinsic mode functions (IMFs) [37] of the monitored structural vibrational signals are abstracted by the EEMD first [38]. Then, specific frequency features in each IMFs are combined and used as the model inputs.

The aim of this study is to test the accuracy and efficiency of a simple framework with shallow architecture using the CGO-ELM model coupled with EEMD for structural damage recognition and compared the performance with existing models such as CNNs with high parameter counts. Compared to common shallow models such as a three-layer ANN, the ELM network is expected to achieve comparable accuracy using shorter training time without the required backpropagation for weight training. The proposed framework provides an alternative yet efficient approach for structural damage recognition and can ensure high-precision recognition performance even in noisy environments.

The rest of the paper is organized as follows: in section 2, we discuss the principle of the CGO-ELM including the preprocessing of

the monitored vibrational signal. In section 3, we demonstrate the working mechanism along with key components and use structural damage data from two classic SHM benchmark models as examples to validate the effectiveness of the proposed framework [39,40]. Section 4 discusses the prediction by CGO-ELM and compares its performance against other existing comment networks. Section 5 is our results and discussions, and Section 6 displays the conclusions.

2. The proposed framework to identify structural damages

2.1. Extreme learning machine (ELM)

In general, neural networks can approximate complex nonlinear mapping relationships between input and output samples. To obtain an accurate result, the weight of the neural network should be well-trained based on different algorithm options such as the backpropagation (BP) [41] and Hidden Markov Model (HMM) [42]. However, these algorithms require a long training time caused by the complex network with thousands of neurons and frequent updates on all weights by the BP algorithm. To overcome this time-consuming issue, Huang et al. pioneered the ELM, a feed-forward neural network having a single layer of hidden nodes [15]. A typical ELM contains only three layers as shown in Fig. 1. Its weights between the input layer and the hidden layer are randomly assigned without any updates during the training stage and the predicting stage. The weights between the hidden layer and the output layer are updated only once by the Moore–Penrose matrix inverse calculation.

This ELM network structure includes n input layer neurons, one hidden layer with L neurons, and one output layer neuron. Assuming there are N input samples (X_i, t_i) , the forward propagation of this ELM is as follows:

$$\sum_{i=1}^L \beta_i g(W_i \cdot X_j + b_i) = o_j, j = 1, \dots, N \quad (1)$$

where $g(x)$ represents the activation function, $W_i = [w_{i,1}, w_{i,2}, \dots, w_{i,n}]^T$ denotes the input weight, β_i is the output weight, and b_i represents the bias of the i th hidden layer neuron.

The objective of the ELM is to minimize the output error, as given in Eq. (2).

$$\sum_{j=1}^N \|o_j - t_j\| = 0 \quad (2)$$

which means the optimal β_i, W_i and b_i can achieve the following goal

$$\sum_{i=1}^L \beta_i g(W_i \cdot X_j + b_i) = t_j, j = 1, \dots, N \quad (3)$$

Eq. (3) can be expressed as a matrix, as shown in Eq. (4)

$$H\beta = T \quad (4)$$

where H denotes the output of the hidden layer neuron,

$$H(W_1, \dots, W_L, b_1, \dots, b_L, X_1, \dots, X_L) = \begin{bmatrix} g(W_1 \cdot X_1 + b_1) & \dots & g(W_L \cdot X_1 + b_L) \\ \vdots & \ddots & \vdots \\ g(W_1 \cdot X_N + b_1) & \dots & g(W_L \cdot X_N + b_L) \end{bmatrix}_{N \times L} \quad (5)$$

β represents the weight of the output, T is the desired output, and m is the output layer neurons.

$$\beta = \begin{bmatrix} \beta_1^T \\ \vdots \\ \beta_L^T \end{bmatrix}_{L \times m} \quad T = \begin{bmatrix} T_1^T \\ \vdots \\ T_N^T \end{bmatrix}_{N \times m} \quad (6)$$

when training the model, the loss function in Eq. (7) is minimized

$$\text{Loss} = \sum_{j=1}^N \left(\sum_{i=1}^L \beta_i g(W_i \cdot X_j + b_i) - t_j \right)^2 \quad (7)$$

the optimal weight of the output $\hat{\beta}$ could be easily calculated by Eq. (8)

$$\hat{\beta} = H^\dagger T \quad (8)$$

where H^\dagger is the Moore-Penrose generalized inverse of matrix H .

Detailed mathematic derivation of the ELM can be referred in Huang et. al. [15].

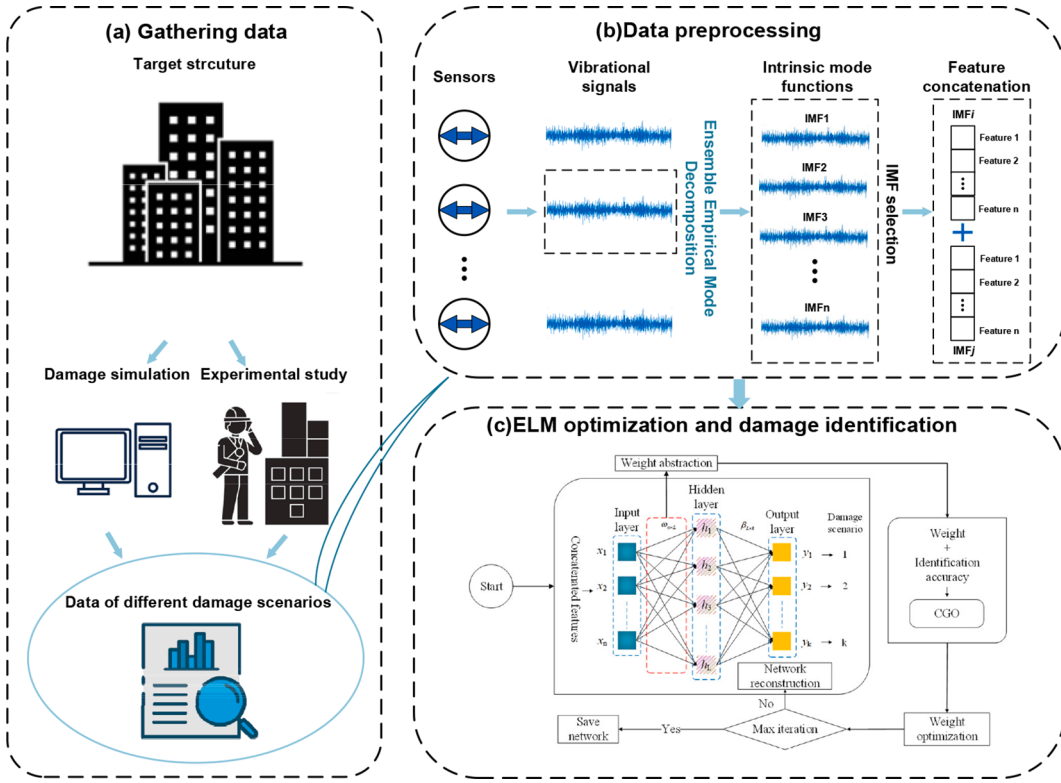


Fig. 2. The proposed CGO-ELM framework for damage identification.

2.2. The general framework using optimized ELM

With a basic understanding of the ELM, we establish a general framework (Fig. 2) to identify structural damage scenarios through vibrational signals. Since the prediction accuracy of the ELM model is not only influenced by the calculated $\hat{\beta}$ but also by the randomly generated W_i , we optimized the W_i using a novel metaheuristic algorithm, see section 2.3 for details. It is essential to extract and employ the representative features from the initial vibrational signals as inputs for the ELM. The utilization of these representative features not only simplifies the complexity of classifier but also guarantees the accuracy of damage identification, see Section 2.4 for details. After sufficient training, the optimized ELM can detect structural damages using new testing data. The accuracy of the damage detector will be evaluated using several indicators; see section 2.5 for details. The proposed framework's effectiveness was demonstrated by utilizing two commonly utilized model structures in the field of structural damage identification. Specifically, these models were the IASC-ASCE SHM benchmark model and the six-story concentrated mass shear structure model [39,40]. The two example model structures and their corresponding damage scenarios will be introduced in Section 3.

2.3. Chaos game optimization

Chaos Game Optimization (CGO) is a metaheuristic algorithm developed for solving optimization problems [23]. It is inspired by chaos theory principles and contains primary patterns such as similar loops, repeated templates, fractals, and multiple sub-systems. From the perspective of the fractals, the CGO generates several potential solutions by first initiating a polygon shape with random points (known solutions), then a series of new points (candidate solutions) are developed through iterations. Similar metaheuristic algorithms have been applied in NNs by replacing the traditionally used Quasi-Newton's method [11], scaled conjugate gradient algorithm [43], or Levenberg-Marquardt algorithm [44] to achieve higher identification accuracy. However, limited studies have integrated this metaheuristic algorithm into ELM. Given the high accuracy and fewer hyperparameters of CGO, we implemented this algorithm in this study as the optimizer of ELM to improve the performance of the CGO-ELM framework.

Mathematically, the candidate solutions of the CGO can be expressed in Eq. (9)

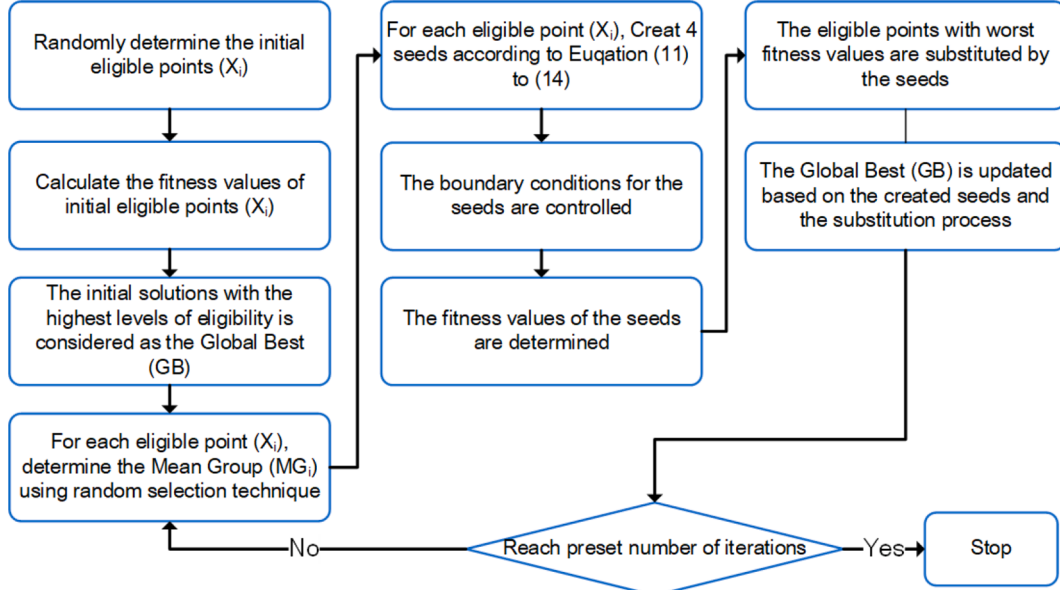


Fig. 3. The flowchart of the CGO algorithm.

$$X = \begin{bmatrix} X_1 \\ X_2 \\ \vdots \\ X_i \\ \vdots \\ X_n \end{bmatrix} = \begin{bmatrix} x_1^1 & x_1^2 & \cdots & x_1^j & \cdots & x_1^d \\ x_2^1 & x_2^2 & \cdots & x_2^j & \cdots & x_2^d \\ \vdots & \vdots & \ddots & \ddots & \ddots & \vdots \\ x_i^1 & x_i^2 & \cdots & x_i^j & \cdots & x_i^d \\ \vdots & \vdots & \ddots & \ddots & \ddots & \vdots \\ x_n^1 & x_n^2 & \cdots & x_n^j & \cdots & x_n^d \end{bmatrix}, \quad \begin{cases} i = 1, 2, \dots, n \\ j = 1, 2, \dots, d \end{cases} \quad (9)$$

where n denotes the number of qualified points (candidate solutions), and d denotes the dimension of the solution. The initial candidate solutions (know solutions) are determined as follows:

$$x_i^j(0) = x_{i,\min}^j + \text{rand.} (x_{i,\max}^j - x_{i,\min}^j), \quad \begin{cases} i = 1, 2, \dots, n \\ j = 1, 2, \dots, d \end{cases} \quad (10)$$

where $x_i^j(0)$ represents the initial position of the qualified point, $x_{i,\min}^j$ and $x_{i,\max}^j$ are the lower and upper bounds in the j th dimension of the i th candidate solution, rand is a random number with interval $[0, 1]$.

In each iteration, bunches of candidate solutions are generated and compared with known solutions, and the one with a better performance replaces the original candidates. After several iterations, all candidate solutions can converge to the same position, which denotes the final optimization result. In this study, the randomly generated $\omega_{n \times L}$ and biases in the ELM are the candidate solutions of the CGO. The 1st iteration of X_i is used as an example to illustrate how the candidate is updated. Specifically, four candidate solutions of $X_i(0)$ are generated, and all five solutions (including $X_i(0)$ itself) are compared. The one that has the worst fitness value is selected as $X_i(1)$. In other words, the candidate $\omega_{n \times L}$ and biases that can achieve the highest identification accuracy in the ELM are saved in $X_i(1)$. Eqs. (11) to (14) show the four candidate solutions, respectively.

$$\text{Seed}_i^1 = X_i + \alpha_i^1 \times (\beta_i^1 \times GB - \gamma_i^1 \times MG_i), \quad i = 1, 2, \dots, n \quad (11)$$

$$\text{Seed}_i^2 = GB + \alpha_i^2 \times (\beta_i^2 \times X_i - \gamma_i^2 \times MG_i), \quad i = 1, 2, \dots, n \quad (12)$$

$$\text{Seed}_i^3 = MG_i + \alpha_i^3 \times (\beta_i^3 \times X_i - \gamma_i^3 \times GB), \quad i = 1, 2, \dots, n \quad (13)$$

$$\text{Seed}_i^4 = X_i (x_i^k = x_i^k + R), \quad k = [1, 2, \dots, d] \quad (14)$$

where X_i is the i th solution candidate of corresponding iteration, i.e., $X_i(0)$; GB is the so far found global best, and MG_i is the mean

values of some selected eligible seeds; a_i is the randomly generated factorial for modelling the movement limitations of the seeds while β_i and γ_i represent a random integer of 0 or 1; the superscript of a_i, β_i and γ_i denote these three values are randomly generated for each seed; k is a random integer in $[1, d]$ interval and R denotes a uniformly distributed random number in $[0, 1]$ interval.

According to a study by Talatahari et al.[\[24\]](#), four different formulations are presented for a_i to control the exploration and exploitation rate of the CGO algorithm, as shown in Eq. [\(15\)](#).

$$\alpha_i = \begin{cases} \text{Rand} \\ 2 \times \text{Rand} \\ (\delta \times \text{Rand}) + 1 \\ (\varepsilon \times \text{Rand}) + (\sim \varepsilon) \end{cases} \quad (15)$$

where Rand is a uniformly distributed random number in the $[0, 1]$ interval; and δ and ε are random integers in the $[0, 1]$ interval, $\sim \varepsilon$ represents a bitwise inverse operation on ε , which means when ε is 0, $\sim \varepsilon$ is 1.

For those solution variables (x_i^j) exceeding the corresponding lower and upper bounds during the iteration, a mathematical flag is defined and a change is applied to these violating variables. After a fixed number of iterations, X_i with the highest accuracy can be found, and the algorithm is terminated. The entire flowchart is given in Fig. [3](#).

2.4. Feature extraction from the vibrational signal

Conventional global structural damage detection methods often rely on using raw or minimally processed vibrational signals to identify structural damage. However, these signals often contain environmental, electromagnetic, and instrumental noise components, which can significantly degrade the accuracy of structural damage identification. To improve the accuracy, it is necessary to introduce a signal preprocessing step to the CGO-ELM framework such as an adaptive time-space analysis method in this study, i.e., the Ensemble Empirical Mode Decomposition (EEMD) [\[45\]](#). EEMD can decompose a complicated signal set into a collection of simple signal subsets called intrinsic mode functions (IMFs) with related residue [\[37\]](#). Different IMFs of the same time-scale dataset reflect the oscillation of the data on different time scales, and the residue reflects the data trend. By filtering those IMFs that have a low correlation with the original signals, the noise in the original signal could be eliminated. In addition, the time and/or frequency features in the IMFs can reflect the structural status concisely and efficiently. Therefore, the features abstracted from IMFs are used to identify structural damage in this study. The following sections introduce how to preprocess the structural vibrational signals using EEMD and the correlated feature extraction procedure.

The specific steps of processing raw signal $x(t)$ using EEMD are as follows:

(1) Acquire the new signal $x_k(t)$ by adding white noise $n_k(t)$ to the raw signal $x(t)$,

$$x_k(t) = x(t) + n_k(t), k = 1, 2, \dots, n \quad (16)$$

where k represents white noise with different noise levels.

(2) Decompose all $x_k(t)$ using the original empirical mode decomposition (EMD) method [\[38\]](#), as shown in Eq. [\(17\)](#)

$$x_k(t) = \sum_{i=1}^m c_{ki}(t) + r_k(t) \quad (17)$$

where $c_{ki}(t)$ is the i th IMF component of $x_k(t)$ obtained from the EMD method, and $r_k(t)$ denotes the corresponding residual.

(3) Calculate the mean value of each IMF order $c_i(t)$, and the mean residual $r(t)$ as follows

$$c_i(t) = \frac{1}{n} \sum_{k=1}^n c_{ki}(t), i = 1, 2, \dots, m \quad (18)$$

$$r(t) = \frac{1}{n} \sum_{k=1}^n r_k(t) \quad (19)$$

(4) The original signal $x(t)$ is expressed as the summation of the $c_i(t)$ and $r(t)$

$$x(t) = \sum_{i=1}^m c_i(t) + r(t) \quad (20)$$

where $c_i(t)$ and $r(t)$ denote the IMFs and residual of $x(t)$ through EEMD, respectively.

After the EEMD of the original signal, each independent IMF component can be obtained. These IMFs reflect the oscillation of the data on different time scales and can be used to describe structure status. However, not all IMFs of the original signal should be used [\[46\]](#). According to studies by Yang et al.[\[46\]](#) and Dong et al.[\[36\]](#), Partial IMFs that can properly represent the original signal are sufficient enough for achieving accurate damage identification and can reduce the complexity of the classifier. Therefore, representative IMFs of the original signal are obtained by correlation analyses in this study. More specifically, the Pearson correlation coefficient of the original signal (e.g., $X = [X_1, X_2, \dots, X_n]$) and its IMF components (e.g., $Y = [Y_1, Y_2, \dots, Y_n]$) are calculated using Eq. [\(21\)](#).

Table 1

Time and frequency features used for the CGO-ELM framework.

Time features		Frequency features	
$X_{ave} = \sum_{i=1}^N X_i / N$	$Cr = X_{peak} / X_{rms}$	$fp_1 = \frac{\sum_{k=1}^K s(k)}{K}$	$fp_6 = \sqrt{\frac{\sum_{k=1}^K (f_k - fp_5)^2 s(k)}{K}}$
$X_{var} = \sum_{i=1}^N (X_i - X_{ave})^2 / N$	$K = \sum_{i=1}^N (X_i - X_{ave})^4 / N X_{std}^4$	$fp_2 = \frac{\sum_{k=1}^K (s(k) - fp_1)^2}{K-1}$	$fp_7 = \sqrt{\frac{\sum_{k=1}^K f_k^2 s(k)}{\sum_{k=1}^K s(k)}}$
$X_{std} = \sqrt{X_{var}}$	$I = X_{peak} / (\sum_{i=1}^N X_i / N)$	$fp_3 = \frac{\sum_{k=1}^K (s(k) - fp_1)^3}{K(\sqrt{fp_2})^3}$	$fp_8 = \sqrt{\frac{\sum_{k=1}^K f_k^4 s(k)}{\sum_{k=1}^K f_k^2 s(k)}}$
$X_{peak} = \max\{ X_i \}$	$S = X_{rms} / (\sum_{i=1}^N X_i / N)$	$fp_4 = \frac{\sum_{k=1}^K (s(k) - fp_1)^4}{K(fp_2)^2}$	$fp_9 = \frac{\sum_{k=1}^K f_k^2 s(k)}{\sqrt{\sum_{k=1}^K s(k) \sum_{k=1}^K f_k^4 s(k)}}$
$X_{rms} = \sqrt{\sum_{i=1}^N X_i^2 / N}$	$Cl = X_{peak} / (\sum_{i=1}^N \sqrt{ X_i } / N)^2$	$fp_5 = \frac{\sum_{k=1}^K f_k s(k)}{\sum_{k=1}^K s(k)}$	$fp_{10} = \frac{fp_6}{fp_5}$

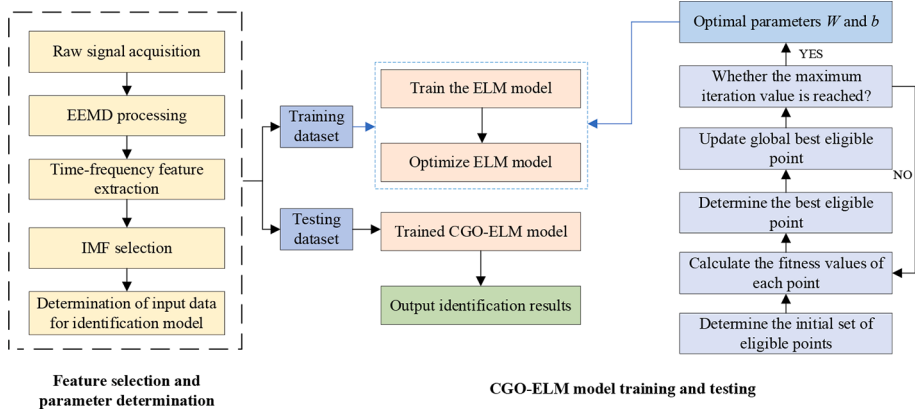


Fig. 4. The proposed damage identification framework.

$$R = \frac{\sum_{i=1}^n (X_i - \bar{X})(Y_i - \bar{Y})}{\sqrt{\sum_{i=1}^n (X_i - \bar{X})^2} \sqrt{\sum_{i=1}^n (Y_i - \bar{Y})^2}} \quad (21)$$

where \bar{X} and \bar{Y} are the mean values of variables X and Y , respectively. Those IMF components that are highly correlated with the original signal are selected to extract vibrational features.

Each selected IMF component consists of a set of time series data. As a result, the corresponding time and/or frequency domain features, calculated using the equations provided in Table 1, can be employed for structural damage identification. In this study, a total of 20 popular time and frequency features [39,47] of each selected IMF are abstracted and combined as the ELM inputs, as shown in Table 1. Detailed IMFs selection and feature combination are introduced in section 4.

2.5. The proposed damage identification framework

The proposed framework starts with employing EEMD to abstract and determine damage features from the raw structural vibrational signal., followed by using the ELM model, with its initial parameters optimized by the CGO algorithm, as the damage detector. Specifically, as shown in Fig. 4, the time and frequency features of the original vibrational signal are abstracted by EEMD and then a specific feature group is selected as the ELM input and split into training and testing sets. The optimal input weights and biases of the ELM are determined by the CGO algorithm, thereby completing the training of the CGO-ELM model. Finally, the testing set is employed to verify the performance of the well-trained CGO-ELM model. The details of the feature selection and parameter determination are introduced in Section 4.

2.6. Evaluation metrics

In order to evaluate the damage identification performance of damage identification methods on structures, three evaluation indicators were used: Precision, Recall, and Accuracy, which are defined as follows.

Actual Damage Scenario				
	A	B	C	
A	10	4	6	Scenario A Precision 50%
B	6	12	6	Scenario B Precision 50%
C	4	4	16	Scenario C Precision 66%
	Scenario A Recall 50%	Scenario B Recall 60%	Scenario C Recall 57%	Overall accuracy 55%

Fig. 5. A representative confusion matrix.

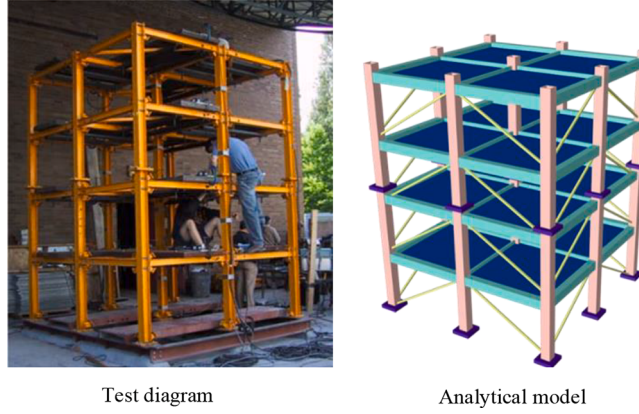


Fig. 6. The IASC-ASCE SHM benchmark structure.

$$\text{Precision} = \frac{\text{TP}}{\text{TP} + \text{FP}} \quad (22)$$

$$\text{Recall} = \frac{\text{TP}}{\text{TP} + \text{FN}} \quad (23)$$

$$\text{Accuracy} = \frac{\text{TP} + \text{TN}}{\text{TP} + \text{TN} + \text{FP} + \text{FN}} = \frac{\text{Number of correct predictions}}{\text{Total number of predictions}} \quad (24)$$

where TP denotes “true positive” standing for the number of samples that are correctly classified into the object class; FP denotes “false positive”, which means the number of samples that are misclassified into the object class; TN represents “true negative”, and it represents the number of samples that belongs to other classes and correctly classified; FN is “false negative”, which implies that the number of samples is misclassified into other classes from the object class.

To intuitively display these indicators, confusion matrices were used in this study, see Fig. 5 for an example. Through this matrix, the actual label and the predicted label of all damage scenarios, and the evaluation metrics are displayed.

3. Case study models

In this study, the effectiveness of the proposed damage identification strategies was tested on two widely used benchmark models, namely the IASC-ASCE SHM benchmark model (referred to as Case 1) and the Six-layer Concentrated Mass Shear Structure Model

Table 2

Description of the damage scenarios.

Damage scenario	Configuration
F0	Without damage
F1	All braces of the first floor are removed
F2	All braces on the first and third floors are removed
F3	A brace on the first floor is removed
F4	A brace is removed from the first and third floors
F5	A brace is removed from the first and second floors
F6	The stiffness of a brace on the first floor is reduced by 30 %

**Fig. 7.** The experimental set-up in An et al. [50].

(referred to as Case 2). These two models have been extensively employed in testing structure damage identification algorithms based on machine learning techniques, making them generic models for damage identification [40,48]. The selected two cases, which are a spatial three-dimensional frame model and a planar frame model respectively, can better verify the generalization performance of the proposed algorithm. The basic parameters and damage scenarios of these two models are described in detail below.

3.1. Case 1: IASC-ASCE SHM benchmark model

In this study, the classic IASC-ASCE SHM benchmark structure [39] is used as an example to validate the effectiveness of the proposed framework due to its popularity in structural damage identification [7,49]. As shown in Fig. 6, it is a 3.6 m tall four-story steel frame structure, with twelve floor beams, nine columns, and eight diagonal braces.

The studied damage scenarios of this case study model are shown in Table 2, and the environmental excitation was used to raise structural vibrational responses. For each damage scenario, a total of 200 structural responses were recorded. 150 of them were used to train the classifier, while the rest were used for testing. The detail of the damage scenarios could be referred to in our previous work in Wang et al. [7].

Table 3
Description of the damage scenarios.

Damage scenario	Configuration
F0	Without damage
F1	The stiffness of the fourth layer is reduced by 20 %
F2	The stiffness of the fifth layer is reduced by 20 %
F3	The stiffness of the fourth layer is reduced by 20 %
F4	The stiffness of the fourth and sixth floors are both reduced by 20 %

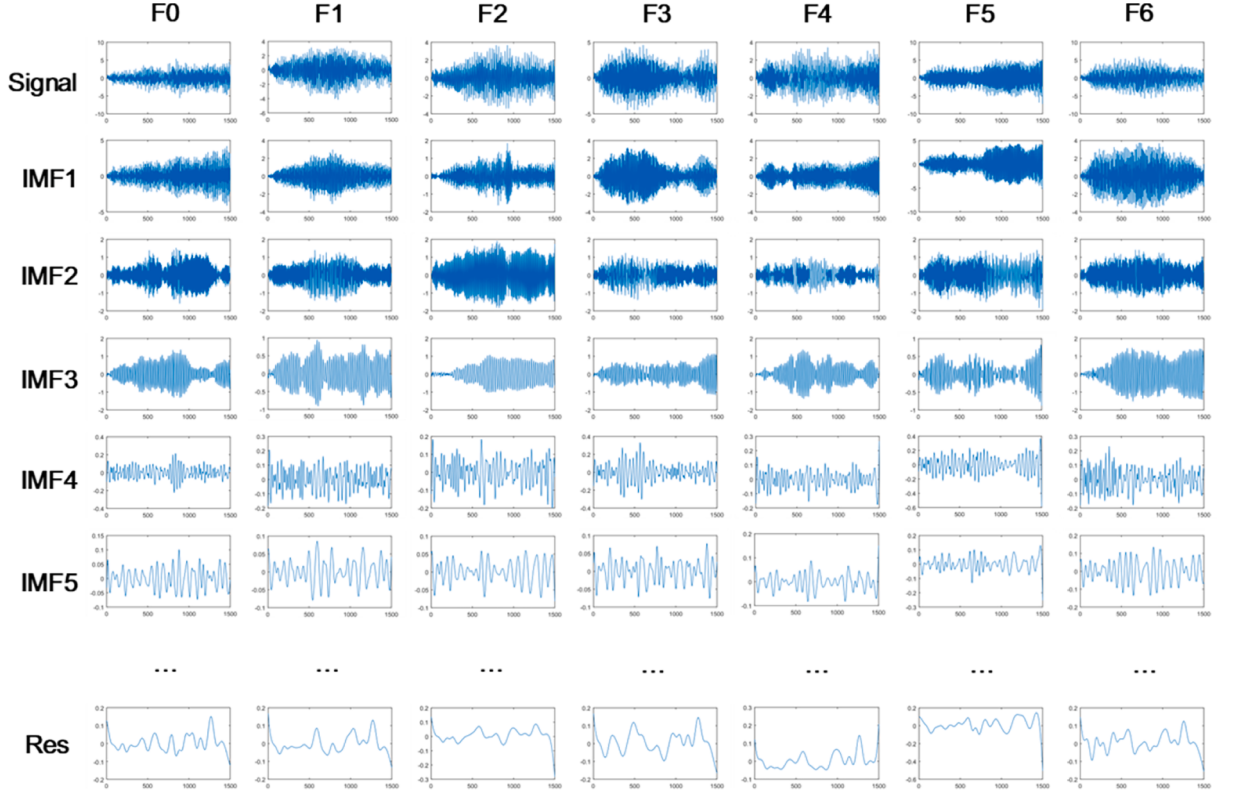


Fig. 8. Damage signal decomposition using EEMD for Case 1.

3.2. Case 2: Six-layer concentrated mass shear structure model

The performance of the proposed damage identification method under single and multiple damage conditions was also verified on a six-story structure using concentrated mass obtained from An et al. [50]. As shown in Fig. 7, the structural model has six identical floors with a width of 260 mm and a height of 210 mm. The concentrated mass of each layer is 21.7 kN, and the cross-sectional size of the column is 50 mm × 1.27 mm.

In this study, three types of damage were considered by changing the stiffness of the column to obtain different damage states, including non-destructive damage, single damage, and multiple damage states. The damage states were numbered according to the degree of damage, as shown in Table 3. It should be noted that the model is excited by white noise during the test. The training and testing samples used for structural damage identification are consistent with the sample sizes mentioned in the previous section, with 150 training samples and 50 testing samples.

4. Optimal parameter determination of the CGO-ELM framework

4.1. Imfs selection

By applying the EEMD to the vibrational responses of different damage scenarios, the corresponding IMFs can be obtained. Fig. 8 and Fig. 9 displays the vibration responses and their representative IMFs for two different damage scenarios, demonstrating unique signal patterns for both the spatial model (Case 1) and the planar model (Case 2), respectively. As the original signal is decomposed

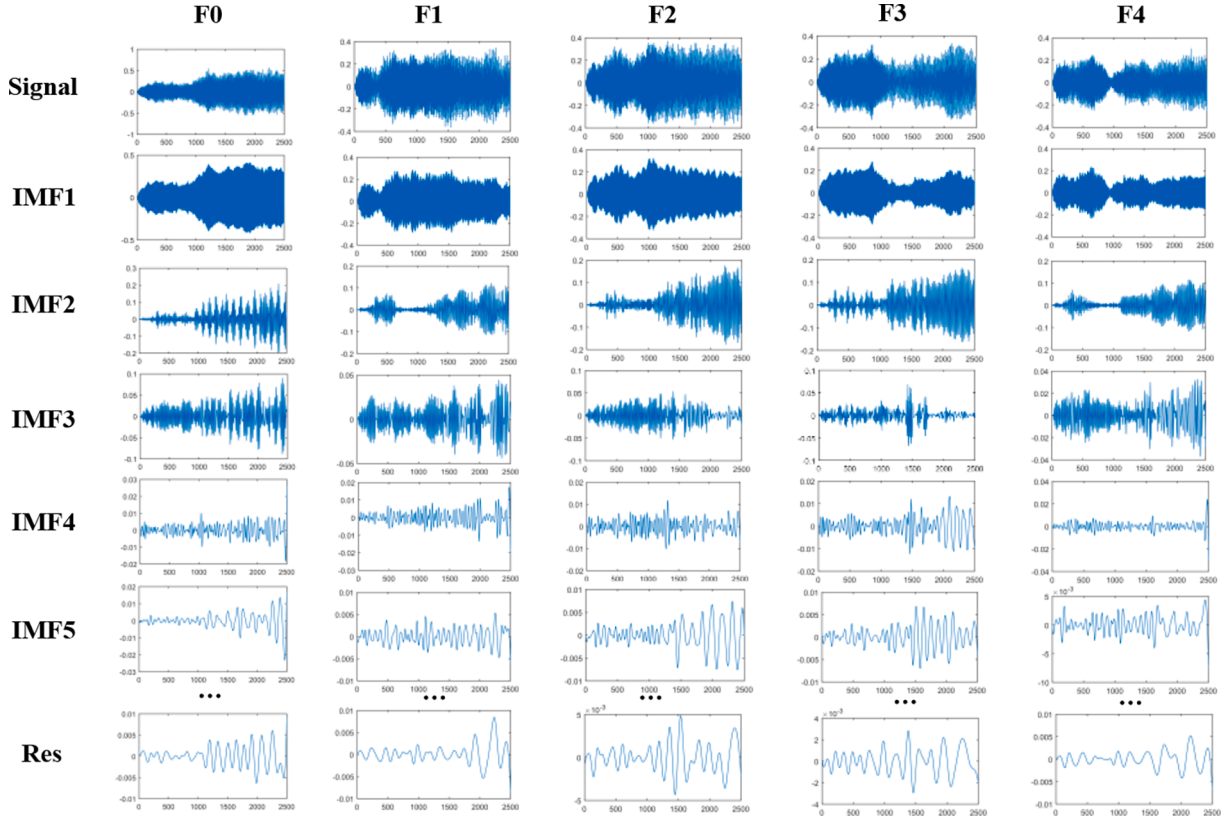


Fig. 9. Damage signal decomposition using EEMD for Case 2.

into representative IMFs of different time scales, their characteristics become more apparent. These representative IMFs of different time scales are sufficient to describe the structural damages, which are highly correlated with the original signal and are selected for further analysis by calculating the Pearson correlation coefficient. The Pearson correlation coefficients between each IMF component and the related original signal are shown in Fig. 10.

Fig. 10 shows that once the decompose order is reaching a threshold level, the correlation coefficient will be getting close to 0, indicating a low reflection of the actual characteristics of the original vibrational signal regardless of specific damage scenarios. In our study, it is coincidental that the corresponding thresholds for both models are their 5th IMF order, and the correlation coefficients for the 6th to 8th IMF order are extremely small. The major difference is that in Case 2, the Pearson correlation coefficients of the IMF components decrease more rapidly, with the Pearson correlation coefficient of its IMF4 component dropping below 0.2, while this phenomenon happens at IMF5 for case 1. This suggests that, compared to Case 1, the higher-order IMF components in Case 2 are less important. Ultimately, IMF1 to IMF5 were selected in sequence for subsequent feature abstraction and combination for both cases.

4.2. Feature combination

For each IMF, different time and frequency features were abstracted according to Table 1. However, previous studies have rarely used those features to identify structural damages, which motivated us to obtain an appropriate feature combination for higher accuracy. To address this issue, the time and frequency features of the original signal were grouped into three sets, including 10-dimensional time features, 10-dimensional frequency features, and 20-dimensional time-frequency features. Features from three groups were inputted into the CGO-ELM framework to identify structural damages.

Table 4 presents a summary of the average accuracy obtained from ten separate tests utilizing various feature sets. Regardless of a spatial frame or a planar frame, the most accurate predictions were obtained using the combination of 10 frequency features. This feature set leads to the highest recognition accuracy and the lowest standard deviation. Therefore, this feature combination was chosen for the CGO-ELM framework.

Along with previously determined IMFs selection, the ten-dimensional frequency features of the first five IMFs are extracted and used as the input for the proposed framework. We also evaluated the influence of data dimension on damage identification accuracy by training the frequency features of IMF1 to IMF5 in various sequences as the damage classifier. The prediction results with five input dimensions are given in Table 5. Increasing the data dimension may not lead to higher prediction accuracy. For Case 1, a trend of increasing and then decreasing is observed as the input data dimension increases. The highest structural damage identification

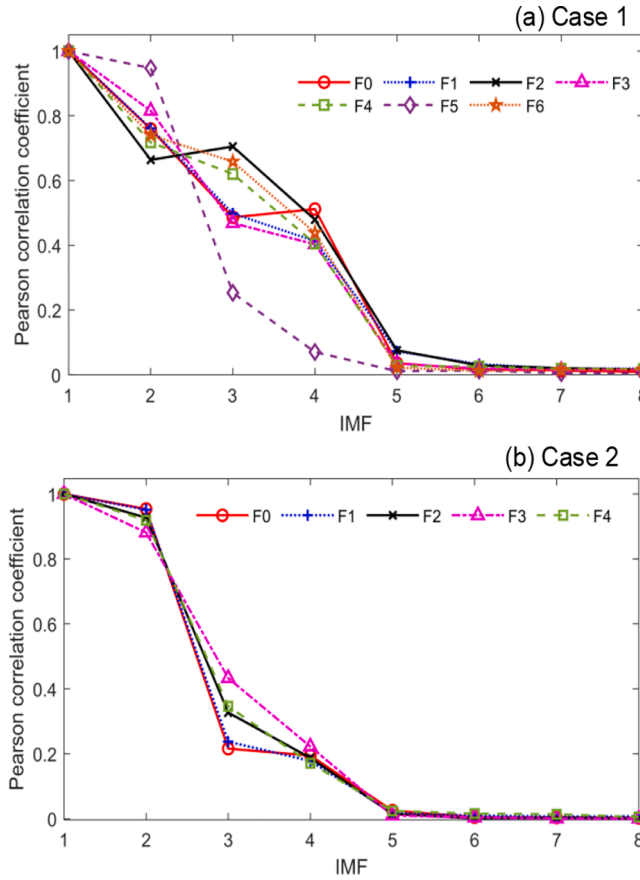


Fig. 10. Pearson correlation coefficient between each IMF component and the original signal.

Table 4
Damage identification accuracy using different feature combinations (Case 1).

Numerical example	Input data	Average accuracy	Standard deviation
Case 1	10-dimensional time features	89.28 % (3125/3500)	0.62
	10-dimensional frequency features	92.74 % (3246/3500)	0.34
	20-dimensional time – frequency features	91.11 % (3189/3500)	0.55
Case 2	10-dimensional time features	87.36 % (2184/2500)	0.96
	10-dimensional frequency features	91.16 % (2279/2500)	0.67
	20-dimensional time – frequency features	90.08 % (2252/2500)	0.83

*3500 = 50 test samples × 7 damage scenarios × 10 tests, 2500 = 50 test samples × 5 damage scenarios × 10 tests.

Table 5
Influence of input dimension on prediction.

Data originality	IMF1	IMF1- IMF2	IMF1- IMF3	IMF1- IMF4	IMF1- IMF5
Input dimension	10	20	30	40	50
Accuracy (%) (Case 1)	94.54	96.57	98.86	98.63	98.23
Accuracy (%) (Case 2)	95.96	97.92	97.44	97.28	97.16

accuracy is achieved by using the first three IMF components (i.e., data dimension of 30) in the three-dimensional frame structure. Therefore, for Case 1, the data dimension selected for input to the machine learning model is 30. Similarly, in Case 2, the highest damage identification accuracy of 97.92 % is achieved by using the first two IMF components (i.e., data dimension of 20), and the damage identification accuracy of the planar frame structure remains essentially unchanged as the input feature dimension increases. Therefore, for the planar frame structure, the input dimension of the machine learning algorithm is 20.

Another key parameter that usually affect the identification accuracy is the number of neurons in the hidden layer. Therefore, we

Table 6

Effect of various hidden layer neurons in the ELM model on damage identification accuracy.

Number of hidden layer neurons	25	30	35	40	45	50
Accuracy (%) (Case 1)	89.83	94.51	98.86	98.94	99.03	99.14
Accuracy (%) (Case 2)	88.32	93.24	97.92	98.48	98.84	99.04

Table 7

Damage identification results using different methods (Case 1).

Model catalog	Shallow Learning Model						Deep Learning Model	
	CGO-ELM	PSO-ELM	SSA-ELM	CGO-ANN	ELM	BP-ANN	Resnet34	GoogLenet
Accuracy (%)	98.86	93.43	96.57	97.86	80.57	84.29	99.14	98.57
Standard deviation	0.23	0.34	0.37	0.85	2.53	2.21	0.19	0.3
Training time/s	31.57	16.43	30.47	58.63	0.21	3.32	123.64	109.89
Testing time/s	0.0036	0.0039	0.0037	0.0043	0.0038	0.0041	5.16	4.58

Table 8

Damage identification results using different methods (Case 2).

Model catalog	Shallow Learning Model						Deep Learning Model	
	CGO-ELM	PSO-ELM	SSA-ELM	CGO-ANN	ELM	BP-ANN	Resnet34	GoogLenet
Accuracy (%)	97.72	93.12	95.64	97.32	81.20	83.48	98.64	98.04
Standard deviation	0.46	0.62	0.58	0.92	1.79	2.13	0.43	0.63
Training time/s	32.03	16.31	30.08	58.90	0.23	3.24	122.97	110.36
Testing time/s	0.0041	0.0037	0.0039	0.0041	0.0037	0.0039	5.21	4.63

compared the model performance using various neuron number (see [Table 6](#)). As shown in the results, in both cases, an increase in the number of neurons leads to improved recognition accuracy. Specifically, with 35 neurons, the recognition accuracy reached approximately 98 %, yielding very satisfactory results. However, as the number of hidden neurons increased from 35 to 50, the prediction accuracy continued to improve (from 98.86 % to 99.14 %), but the magnitude of increase significantly diminished. To elaborate, when the number of neurons changed from 25 to 35, the increase in prediction accuracy was 9.03 %. In contrast, when the number of neurons changed from 35 to 50, the increase in prediction accuracy was only 0.28 %.

5. Results and discussions

5.1. Performance of CGO-ELM against other ML models

To validate and assess the effectiveness of the CGO-ELM framework proposed in this study, conventional machine-learning models were also implemented, utilizing identical training and testing datasets. These models were run ten iterations, and the results were used as the control group. The results are given in [Tables 7](#) and [Table 8](#). The shallow learning models include ELM and the most widely used neural network, i.e., the three-layer artificial neural network (ANN) [51]. Similar to the ELM model, the BP-ANN algorithm comprises three layers: an input layer, a hidden layer, and an output layer. For Case 1, the input and output layers of the BP-ANN have 30 and 7 neurons, respectively. Through testing, it was found that setting the number of neurons in the hidden layer to 45 that could result in better classification performance. Additionally, the learning rate is set to 0.1, the number of iterations is 1000, and the batch size is 16. The weight parameters of ELM and ANN were optimized by several metaheuristic-algorithm including CGO, PSO [52], and sparrow search algorithm (SSA) [53]. In addition, the classic gradient-based method, i.e., the back-propagation (BP) [16] method, was also evaluated to optimize the modal weights for comparison. For deep learning models, two high-efficient neural networks, i.e., the GoogLeNet [54] and the ResNet [14] were investigated for comparative study. These two neural networks have achieved bunches of progress in classification-related research, and are good benchmarks to evaluate the performance of the proposed damage identification model. All simulations were executed on a personal laptop with an AMD Ryzen-7 5800H processor (3.20 GHz) with 16 GB RAM.

It can be seen from [Table 7](#) that: (1) The proposed CGO-ELM with a damage identification accuracy above 97 % outperforms the widely used ELM and BP-ANN (both are below 85 %). (2) Among models using the ELM, the proposed CGO-ELM method achieved the highest accuracy for damage identification compared to the predictions by PSO-ELM and SSA-ELM. (3) The CGO-ANN model showed a similar identification accuracy to the CGO-ELM model but nearly doubled the training time. The reason for a longer training time in ANN is that more layers of weight parameters must be optimized compared to the ELM. (4) Deep learning models performed as excellent as the CGO-ELM model but needed higher training time, yet the testing time of the CGO-ELM model is just about 0.10 % of two widely-used deep networks. Overall, the proposed CGO-ELM framework is able to achieve high accuracy and efficiency simultaneously.

[Table 8](#) shows the identification performance of the Six-layer Concentrated Mass Shear Structure Model under different damage

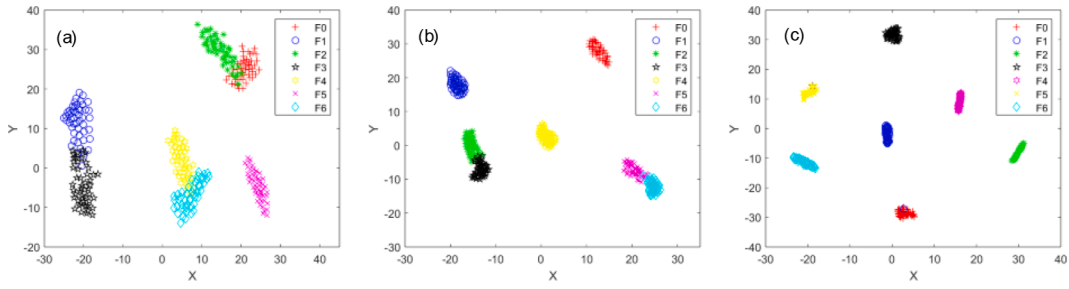


Fig. 11. Clustering results before and after processing EEMD frequency domain features with the proposed optimized ELM model. (a) original frequency domain signals. (b) output signals of ELM's hidden layer. (c) hidden layer output signals of the proposed CGO-ELM.

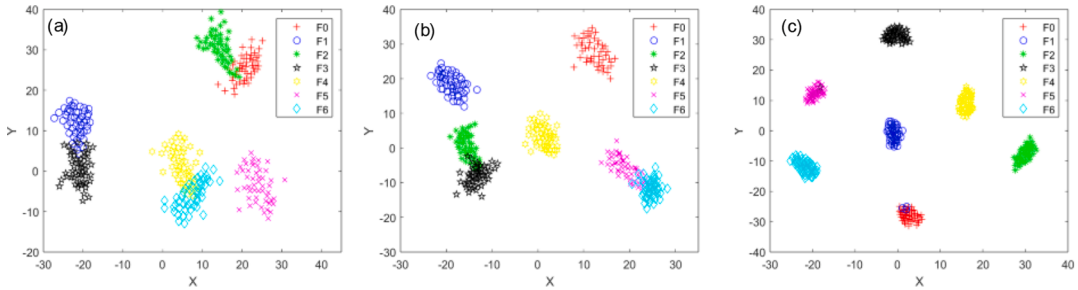


Fig. 12. Clustering results before and after processing EEMD frequency domain features with the proposed optimized ELM model under noisy conditions. (a) original frequency domain signals. (b) output signals of ELM's hidden layer. (c) hidden layer output signals of the proposed CGO-ELM.

identification algorithms. Similarly, it can be observed that the proposed CGO-ELM algorithm achieves an accuracy of 97.72 % in damage identification, ranking third among all the compared algorithms, only slightly lower than the accuracies of two deep learning models, which are 98.64 % and 98.04 %, respectively. Besides, the proposed algorithm has a clear advantage in terms of model training and testing time. Specifically, the training time of the CGO-ELM algorithm is around 25 % of that of deep learning models, and the testing time of the proposed algorithm can be completed within 1 s. This indicates that the damage identification performance in both Case 1 and Case 2 follows similar patterns and highlights the significant advantage of the proposed algorithm in terms of training and testing speed.

We conducted clustering analysis by considering whether it was proceed by the ELM to showcase the significance of the ELM model. Specifically, we clustered the frequency domain features of the raw data after EEMD processing. We performed clustering analysis on the outputs of the hidden layer of the ELM model when processing these frequency domain features. As an example, for Case 1, we present the feature clustering results in both noise-free and noisy conditions (SNR at 40 dB), as illustrated in Figs. 11 and 12.

Based on Fig. 11(a), it is obvious that the original frequency domain signals exhibit a significant misclassification issue, with all but the F5 damage type showing instances of misclassification among the other six damage types. The clustering results for various feature sets, as seen in Fig. 11(b) and Fig. 11(c) after ELM's hidden layer feature extraction, appear quite scattered. This indicates that after ELM processing, the features of different damage signals are strengthened, enabling better distinction and clustering. In addition, Fig. 11(c) demonstrates that only two samples are misclassified, which is fewer than the misclassification observed in Fig. 11(b), highlighting the advantages of CGO-optimized ELM. Fig. 12 represents the feature clustering results in the presence of noise. Compared to Fig. 11, it mainly reveals two characteristics. First, the sample distribution for all three clustering scenarios is somewhat more dispersed. Second, the overall performance is weaker compared to the noise-free conditions, but CGO-ELM remains the best-performing method. Thus, it is clear that ELM plays a role in enhancing feature discrimination, with CGO-ELM's impact being more pronounced.

5.2. Anti-noise analysis

Having proved the effectiveness of the proposed framework, it is necessary to investigate the performance of the CGO-ELM model using noisy data. In this study, Gaussian white noise data with different levels were inserted into the original data, and the magnitude of noise is expressed by the signal-to-noise ratio (SNR), as shown in Eq. (25).

$$\text{SNR}(\text{db}) = 20 \log_{10} \frac{A_{\text{signal}}}{A_{\text{noise}}} \quad (25)$$

where $A_{\text{signal}}/A_{\text{noise}}$ represents the root mean squares of the clean response/ noise. Details of how the noise is introduced could be refer

Table 9

The average damage identification accuracy (%) of different methods under noises.

Mode 1	SNR	CGO-ELM	SSA-ELM	PSO-ELM	ELM	CGO-ANN	BP-ANN	Resnet34	Goog–Lenet
Case 1	60 dB	98.28	96.14	92.57	80.29	96.83	82.54	98.74	97.86
	55 dB	96.94	95.36	91.23	79.56	96.14	81.14	97.91	97.00
	50 dB	96.47	93.98	90.86	78.28	95.29	79.03	96.91	96.03
	45 dB	96.03	92.16	89.16	77.13	93.83	77.29	95.86	94.89
	40 dB	95.15	91.4	88.42	76.21	92.89	74.89	94.43	93.60
	35 dB	94.26	90.01	87.28	74.93	92.74	72.43	92.94	92.14
	30 dB	93.78	89.04	86.43	73.21	92.03	70.71	91.49	90.43
	25 dB	93.08	87.17	85.63	71.09	90.23	68.86	89.91	88.51
	20 dB	92.67	84.65	83.14	68.71	87.23	67.23	88.14	86.71
	15 dB	97.28	95.64	92.88	81.56	96.28	82.88	97.92	97.52
Case 2	55 dB	96.72	94.32	91.96	80.72	95.72	81.48	97.21	96.72
	50 dB	96.36	93.28	91.08	79.64	95.04	79.96	96.20	95.76
	45 dB	96.04	92.64	89.04	78.52	94.40	78.20	95.12	94.64
	40 dB	95.52	91.48	87.40	77.16	93.64	76.20	93.96	93.20
	35 dB	94.84	90.12	86.28	75.24	91.84	73.92	92.80	91.60
	30 dB	93.68	88.84	85.36	73.28	90.32	71.80	91.56	89.92
	25 dB	92.84	86.36	84.20	71.00	88.92	69.20	90.20	88.08
	20 dB	91.88	83.08	82.16	68.12	86.44	66.80	88.52	86.32

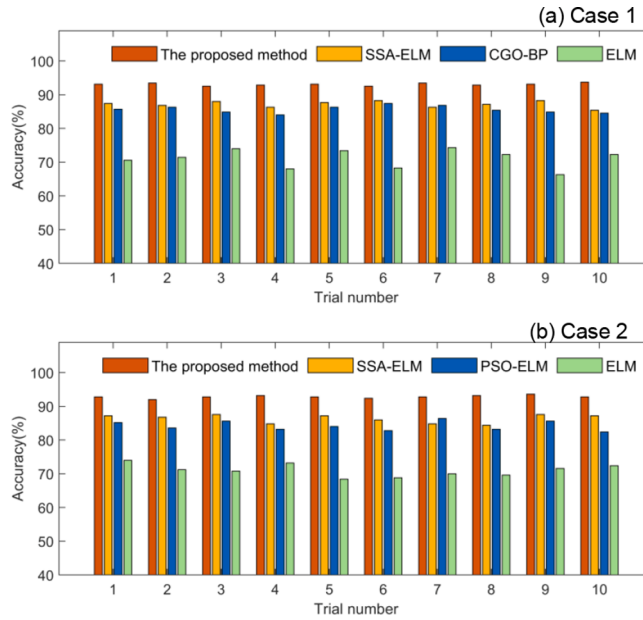


Fig. 13. Identification accuracy of different trials when SNR equals 25 dB.

to [55].

Specifically, nine SNRs ranging from 20 dB to 60 dB were considered (the higher the SNR, the lower the noise level), and a total of ten analyses in each SNR were conducted for the proposed CGO-ELM and other methods. The results are displayed in Table 9.

Table 9 shows that in Case 1, the damage identification accuracy of the proposed CGO-ELM framework maintained an excellent level with identification accuracy above 92 % under high-noise environments (SNR below 30 dB). As SNR reduced to 20 dB, only a 5.61 % reduction was found compared with the model in minor noise conditions (SNR 60 dB), while the others all decreased at least by 9.43 %. The proposed CGO-ELM framework not only demonstrates excellent noise resistance but also showcase a high consistency for ten trials when the SNR equals 25 dB. Similarly, in Case 2, the recognition accuracy of CGO-ELM decreased from 97.28 % to 91.88 % (a decrease of 5.4 %) as the noise level increased. But the recognition accuracy of ELM, PSO-ELM, and SSA-ELM has decreased more, at least decreased by 10.72 %. In addition, compared to shallow learning methods based on ANN (i.e., CGO-ANN and BP-ANN) and commonly used deep learning methods (i.e., Resnet and GoogLenet), the proposed CGO-ELM shows better noise robustness. The accuracy of CGO-ANN decreased by 9.6 % from 96.83 % to 87.23 %, and the accuracy of BP-ANN decreased by 15.31 % from 82.54 % to 67.23 %. It shows that the accuracy of these two methods decreased more than that of the proposed CGO-ELM. While Resnet34 and GoogLenet perform well in low-noise scenarios, their effectiveness significantly diminishes as noise levels rise. In contrast, as noise levels increase, CGO-ELM demonstrates superior noise resistance compared to these deep learning models. When SNR changes from 60

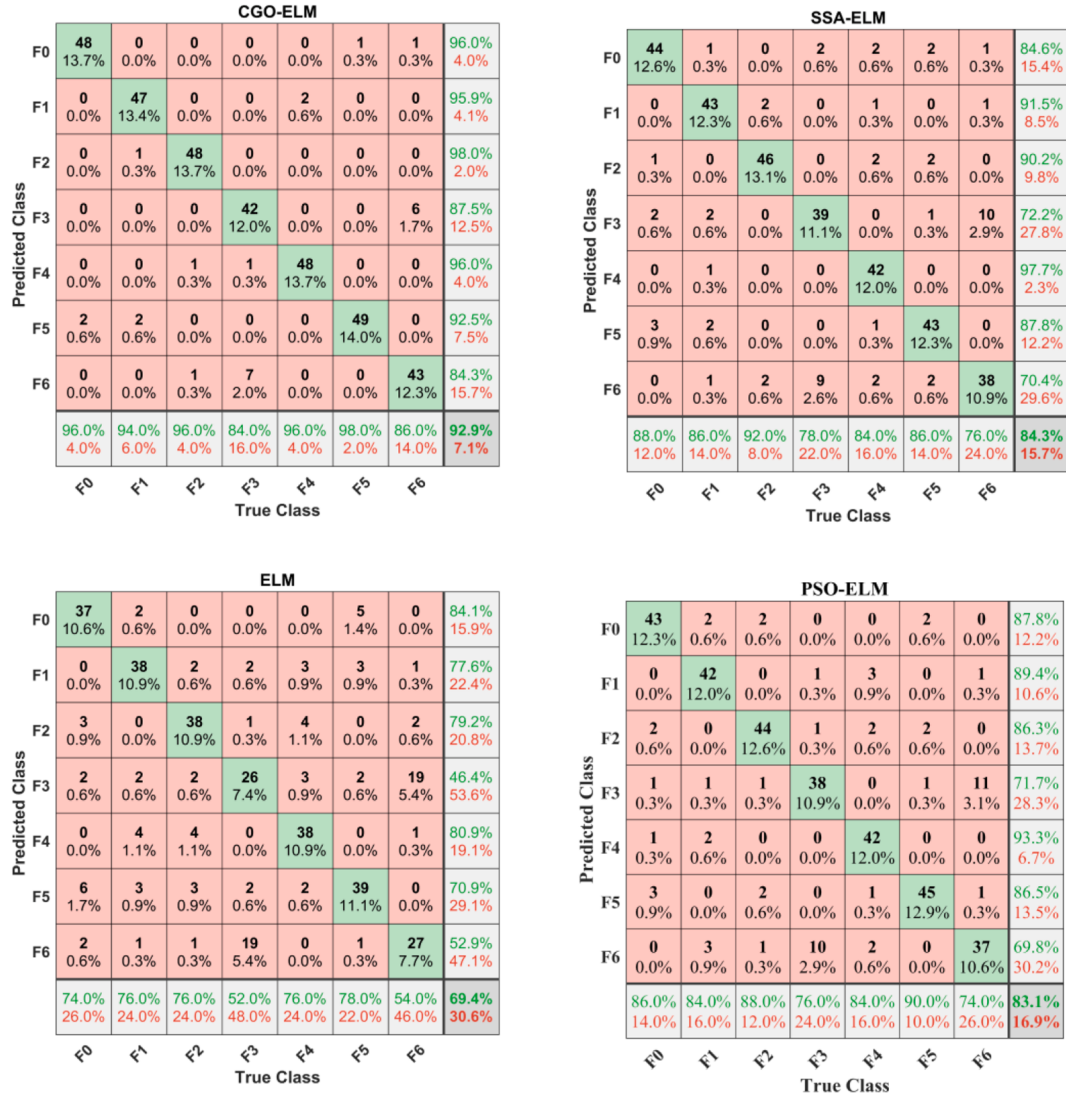


Fig. 14. The confusion matrices of different methods when SNR equals 20 dB (Case 1).

dB to 20 dB, the damage detection accuracy of the proposed method decreases by only 5.61 % as mentioned above, which is smaller than that of Resnet34 (10.6 %) and GoogLenet (11.15 %). Meanwhile, for Case 1 in Table 9 with the highest noise level (i.e., SNR of 20 dB), the recognition accuracy of CGO-ELM is 92.67 %, which is higher than that of Resnet34 (88.14 %) and GoogLenet (86.71 %). Overall, the similar trends observed in both cases indicate that the proposed algorithm has good noise robustness compared to other algorithms, no matter whether the tested structure is a three-dimensional structure or a planar frame. The above results have shown that compared with other shallow learning methods (such as CGO-ANN and BP-ANN) and commonly used deep learning methods (such as Resnet and GoogLenet), the improved ELM based methods (including CGO-ELM, PSO-ELM, SSA-ELM) have demonstrated their capabilities. Thus, only the ELM-based methods were carefully compared and studied in the following sections.

Fig. 13 indicates an accurate and stable performance by the CGO-ELM framework for damage identification. In the case of a signal-to-noise ratio of 25 dB, the proposed method achieves the highest identification accuracy and the smallest fluctuation in accuracy among 10 damage identifications, which is significantly better than the other three algorithms. To further compare the robustness of these four methods under high SNR levels, Fig. 14 shows four confusion matrices in the same trial analysis for Case 1 when the SNR equals 20 dB. It can be observed that regardless of the specific damage scenarios, the CGO-ELM has the highest identification accuracy. But it should be noted that all four models show poor prediction for damage scenarios F3 (a brace on the first floor is removed) and F6 (The stiffness of a brace on the first floor is reduced by 30 %) and even the CGO-ELM model cannot reach a 90 % identification accuracy. The reason for the poor prediction is that compared with other damage scenarios, F3 and F6 share similar damage conditions in which total or partial damage of a brace happened on the first floor. Their monitored vibrational signals may contain indistinguishable damage features, leading to mutual misclassification and corresponding low identification accuracy.

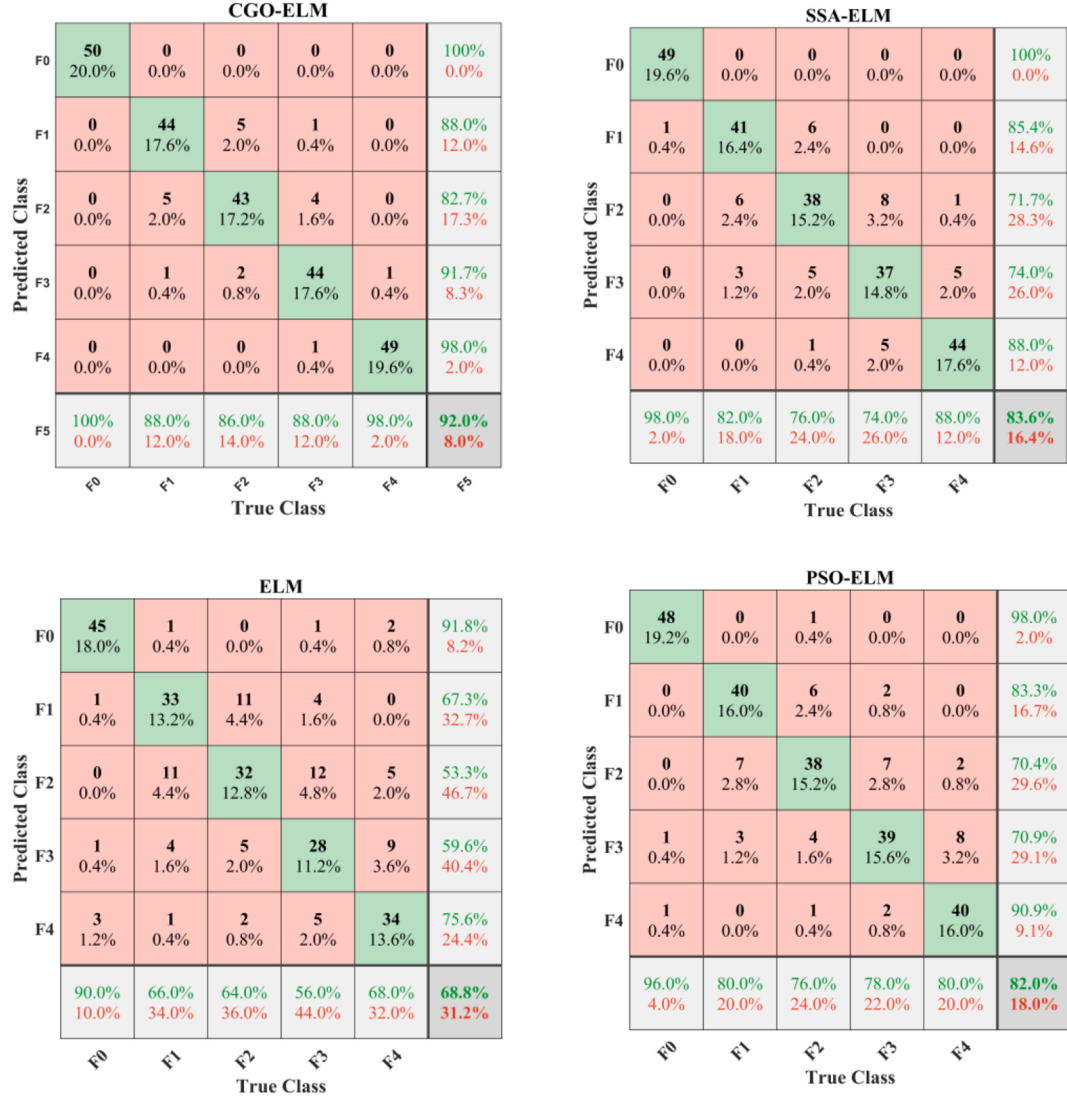


Fig. 15. The confusion matrices of different methods when SNR equals to 20 dB (Case 2).

Similarly, Fig. 15 shows the confusion matrices of CGO-ELM, SSA-ELM, PSO-ELM, and ELM for Case 2 in a single test when the SNR is 20 dB. Consistent with the results of Case 1, the proposed algorithm exhibits the highest accuracy in damage identification and significant advantages in noise resistance. However, unlike Case 1, it can be observed from the confusion matrix in Fig. 15 that the misclassification of samples belonging to damage types F1 and F2 is more frequent in Case 2. The main reason is that the IMF1 components of the samples in F1 and F2 have high similarity, possibly due to their adjacent locations in the structure (layers 4 and 5, respectively), leading to similar changes in structural stiffness and consequently causing misclassification of damage types. Nevertheless, the proposed algorithm achieves excellent identification performance and anti-noise feature compared to the other three algorithms for both planar and spatial model.

6. Conclusion

This study proposes a high-speed and simple-implement damage identification framework based on an extreme learning machine (ELM) coupled with chaos game optimization (CGO). The inputs of this method were obtained by performing ensemble empirical mode decomposition (EEMD) to the structural vibrational signals. Following a series of analyses, we determined the optimal input dimension, selected features, and hidden layer neuron numbers for the proposed CGO-ELM framework. Then, the performance of the proposed framework was validated by both special and planar structures under noise-free and noise-contaminated conditions. Our results show that using metaheuristic algorithms to optimize the weights of the ELM is an effective method to improve its damage identification accuracy. Compared with shallow learning models using PSO and SSA, the CGO-ELM model achieved the highest

accuracy for damage identification. The proposed method also outperformed deep learning methods such as GoogLeNet and Resnet with similar identification accuracy yet requires no more than one-third of the training time and 1 % of testing time. Under noisy conditions, the proposed CGO-ELM framework exhibited outstanding high accuracy, fast computational speed, and strong noise resistance in damage identifications. Despite the excellent performance using the CGO-ELM framework, the CGO optimization algorithm is not suitable for optimizing deep learning models, which would cost consumes large computing resources due to a large number of model network parameters. Further investigations can be done on conducting sensitivity analysis and integrating multiple learning techniques to improve the robustness of the framework. We believe that this method can be coupled with advanced structural sensing techniques in developing next-generation structural monitoring systems, and improve the autonomous level when building smart cities.

It is essential to note that this study is based on simple scaled models for collecting structural vibration signals, which differ from real structures. Due to practical considerations, it is currently challenging to fully destroy existing engineering structures for relevant analyses. However, it can be anticipated that with the development of the finite element method, numerical models can accurately simulate actual structural damage. At that point, using new data to train the structural damage identification model proposed in this paper will enable judgments about the damage conditions of real structures. Therefore, this method holds the potential for beneficial applications in engineering.

CRediT authorship contribution statement

Xinwei Wang: Writing – review & editing, Writing – original draft, Visualization, Methodology, Investigation, Formal analysis, Conceptualization. **Yinghao Zhao:** Formal analysis, Conceptualization, Investigation, Validation, Writing – original draft, Writing – review & editing. **Zhihao Wang:** Formal analysis, Investigation, Visualization. **Nan Hu:** Writing – review & editing, Writing – original draft, Supervision, Resources.

Declaration of competing interest

The authors declare that they have no known competing financial interests or personal relationships that could have appeared to influence the work reported in this paper.

Data availability

Data will be made available on request.

Acknowledgment

X. W. and Y. Z. contributed equally to this work. This work was supported by the Science and Technology Plan Project of the Guangzhou Municipal Construction Group Co., Ltd (No.2021KJ005) and the Guangdong Provincial Key Laboratory of Modern Civil Engineering Technology (2021B1212040003).

References

- [1] Y. Zhao, Q. Yan, Z. Yang, X. Yu, B. Jia, A novel artificial bee colony algorithm for structural damage detection, *Adv. Civil Eng.* (2020) 3743089.
- [2] X. Kong, C.S. Cai, J. Hu, The state-of-the-art on framework of vibration-based structural damage identification for decision making, *Appl. Sci.* 7 (5) (2017) 497.
- [3] W.Y. He, S. Zhu, W.-X. Ren, Two-phase damage detection of beam structures under moving load using multi-scale wavelet signal processing and wavelet finite element model, *App. Math. Model.* 66 (2019) 728–744.
- [4] A.H. Alavi, H. Hasni, N. Lajnef, K. Chatti, F. Faridazar, An intelligent structural damage detection approach based on self-powered wireless sensor data, *Autom. Constr.* 62 (2016) 24–44.
- [5] M.A. Perez, L. Gil, S. Oller, Impact damage identification in composite laminates using vibration testing, *Compos. Struct.* 108 (2014) 267–276.
- [6] S.D. Fassio, J.S. Sakellariou, Time-series methods for fault detection and identification in vibrating structures, *Philos. Trans. R. Soc. A Math. Phys. Eng. Sci.* 365 (1851) (2007) 411–448.
- [7] X. Wang, M.M. Shahzad, A novel structural damage identification scheme based on deep learning framework, *Elsevier, Structures*, 2021, pp. 1537–1549.
- [8] H. Kim, C. Jin, M. Kim, K. Kim, Damage detection of bottom-set gillnet using artificial neural network, *Ocean Eng.* 208 (2020) 107423.
- [9] M. Gul, F.N. Catbas, Statistical pattern recognition for Structural Health Monitoring using time series modeling: Theory and experimental verifications, *Mech. Syst. Sig. Process.* 23 (7) (2009) 2192–2204.
- [10] A.M. Ay, Y. Wang, Structural damage identification based on self-fitting ARMAX model and multi-sensor data fusion, *Struct. Health Monit.* 13 (4) (2014) 445–460.
- [11] Y. Zhao, H. Hu, C. Song, Z. Wang, Predicting compressive strength of manufactured-sand concrete using conventional and metaheuristic-tuned artificial neural network, *Measurement* 194 (2022) 110993.
- [12] L.K. Foong, Y. Zhao, C. Bai, C. Xu, Efficient metaheuristic-retrofitted techniques for concrete slump simulation, *Smart Struct. Syst., Int. J.* 27 (5) (2021) 745–759.
- [13] Z. Jia, S. Wang, K. Zhao, Z. Li, Q. Yang, Z. Liu, An efficient diagnostic strategy for intermittent faults in electronic circuit systems by enhancing and locating local features of faults, *Meas. Sci. Technol.* 35 (2024) 036107.
- [14] K. He, X. Zhang, S. Ren, J. Sun, Deep residual learning for image recognition, in: *Proceedings of the IEEE Conference on Computer Vision and Pattern Recognition*, 2016, pp. 770–778.
- [15] G.-B. Huang, Q.Y. Zhu, C.-K. Siew, Extreme learning machine: theory and applications, *Neurocomputing* 70 (1–3) (2006) 489–501.
- [16] Y. Zhao, H. Moayed, M. Bahraei, L.K. Foong, Employing TLBO and SCE for optimal prediction of the compressive strength of concrete, *Smart Struct. Syst.* 26 (6) (2020) 753–763.
- [17] H. Moayed, B. Kalantar, L.K. Foong, D. Tien Bui, A. Motavalli, Application of three metaheuristic techniques in simulation of concrete slump, *Appl. Sci.* 9 (20) (2019) 4340.

- [18] H. Safayenikoo, F. Nejati, M.L. Nehdi, Indirect Analysis of Concrete Slump Using Different Metaheuristic-Empowered Neural Processors, *Sustainability* 14 (16) (2022) 10373.
- [19] M.A. Ehyaei, M. Tahani, P. Ahmadi, M. Esfandiari, Optimization of fog inlet air cooling system for combined cycle power plants using genetic algorithm, *Appl. Therm. Eng.* 76 (2015) 449–461.
- [20] H. Moayedi, M. Mehrabi, M. Mosallanezhad, A.S.A. Rashid, B. Pradhan, Modification of landslide susceptibility mapping using optimized PSO-ANN technique, *Eng. Comput.* 35 (3) (2019) 967–984.
- [21] G. Zhou, H. Moayedi, M. Bahiraei, Z. Lyu, Employing artificial bee colony and particle swarm techniques for optimizing a neural network in prediction of heating and cooling loads of residential buildings, *J. Clean. Prod.* 254 (2020) 120082.
- [22] H. Moayedi, A. Rezaei, An artificial neural network approach for under-reamed piles subjected to uplift forces in dry sand, *Neural Comput. & Applic.* 31 (2) (2019) 327–336.
- [23] S. Talatahari, M. Azizi, Chaos Game Optimization: a novel metaheuristic algorithm, *Artif. Intell. Rev.* 54 (2) (2021) 917–1004.
- [24] S. Talatahari, M. Azizi, Optimization of constrained mathematical and engineering design problems using chaos game optimization, *Comput. Ind. Eng.* 145 (2020) 106560.
- [25] H. Zheng, A. Mita, Localized damage detection of structures subject to multiple ambient excitations using two distance measures for autoregressive models, *Struct. Health Monit.* 8 (3) (2009) 207–222.
- [26] Y. Kim, J. Kim, Y.H. Kim, J. Chong, H.S. Park, System identification of smart buildings under ambient excitations, *Measurement* 87 (2016) 294–302.
- [27] C. Bao, H. Hao, Z.X. Li, Integrated ARMA model method for damage detection of subsea pipeline system, *Eng. Struct.* 48 (2013) 176–192.
- [28] A.A. Mousavi, C. Zhang, S.F. Masri, G. Gholipour, Structural damage localization and quantification based on a CEEMDAN Hilbert transform neural network approach: a model steel truss bridge case study, *Sensors* 20 (5) (2020) 1271.
- [29] W.L. Bayissa, N. Haritos, M. Sofi, Comparative study of broadband damage localization methods applied to test data, *Ocean Eng.* 38 (2–3) (2011) 329–340.
- [30] B. Ghahremani, M. Bitaraf, A.K. Ghorbani-Tanha, R. Fallahi, Structural damage identification based on fast S-transform and convolutional neural networks, *Elsevier, Structures*, 2021, pp. 1199–1209.
- [31] Z. Chen, R. Zhang, J. Zheng, H. Sun, Sparse Bayesian learning for structural damage identification, *Mech. Syst. Sig. Process.* 140 (2020) 106689.
- [32] S. Mangalathu, S.H. Hwang, E. Choi, J.S. Jeon, Rapid seismic damage evaluation of bridge portfolios using machine learning techniques, *Eng. Struct.* 201 (2019) 109785.
- [33] Y.-M. Hsueh, V.R. Ittangihal, W.-B. Wu, H.C. Chang, C.C. Kuo, Fault diagnosis system for induction motors by CNN using empirical wavelet transform, *Symmetry* 11 (10) (2019) 1212.
- [34] L. Wen, L. Gao, X. Li, M. Xie, G. Li, A new data-driven intelligent fault diagnosis by using convolutional neural network, in: 2017 IEEE International Conference on Industrial Engineering and Engineering Management (IEEM), 2017, pp. 813–817.
- [35] Y. Zhang, Y. Miyamori, S. Mikami, T. Saito, Vibration-based structural state identification by a 1-dimensional convolutional neural network, *Comput. Aided Civ. Inf. Eng.* 34 (9) (2019) 822–839.
- [36] X. Dong, J. Lian, H. Wang, Vibration source identification of offshore wind turbine structure based on optimized spectral kurtosis and ensemble empirical mode decomposition, *Ocean Eng.* 172 (2019) 199–212.
- [37] Y. Zhang, J. Lian, F. Liu, An improved filtering method based on EEMD and wavelet-threshold for modal parameter identification of hydraulic structure, *Mech. Syst. Sig. Process.* 68 (2016) 316–329.
- [38] Z. Wu, N.E. Huang, Ensemble empirical mode decomposition: a noise-assisted data analysis method, *Adv. Adapt. Data Anal.* 1 (01) (2009) 1–41.
- [39] E.A. Johnson, H.F. Lam, L.S. Katafygiotis, J.L. Beck, Phase I IASC-ASCE structural health monitoring benchmark problem using simulated data, *J. Eng. Mech.* 130 (1) (2004) 3–15.
- [40] H. Zhu, H. Yu, F. Gao, S. Weng, Y. Sun, Q. Hu, Damage identification using time series analysis and sparse regularization, *Struct. Control Health Monit.* 27 (9) (2020) e2554.
- [41] Y. LeCun, D. Touresky, G. Hinton, T. Sejnowski, A theoretical framework for back-propagation, in: Proceedings of the 1988 Connectionist Models Summer School, 1988, pp. 21–28.
- [42] S. Fine, Y. Singer, N. Tishby, The hierarchical hidden Markov model: Analysis and applications, *Mach. Learn.* 32 (1) (1998) 41–62.
- [43] M.F. Møller, A scaled conjugate gradient algorithm for fast supervised learning, *Neural Netw.* 6 (4) (1993) 525–533.
- [44] J. de Jesús Rubio, Stability analysis of the modified Levenberg–Marquardt algorithm for the artificial neural network training, *IEEE transactions on neural networks and learning systems* 32(8) (2020) 3510–3524.
- [45] J. Zhang, R. Yan, C. Yang, Structural modal identification through ensemble empirical modal decomposition, *Smart Struct. Syst.* 11 (1) (2013) 123–134.
- [46] J. Yang, F. Yang, Y. Zhou, D. Wang, R. Li, G. Wang, W. Chen, A data-driven structural damage detection framework based on parallel convolutional neural network and bidirectional gated recurrent unit, *Inf. Sci.* 566 (2021) 103–117.
- [47] J. Zhang, R. Jiang, B. Li, N. Xu, An automatic recognition method of microseismic signals based on EEMD-SVD and ELM, *Comput. Geosci.* 133 (2019) 104318.
- [48] Y. An, B.F. Spencer Jr, J. Ou, Real-time fast damage detection of shear structures with random base excitation, *Measurement* 74 (2015) 92–102.
- [49] H. Hashim, Z. Ibrahim, H.A. Razak, Dynamic characteristics and model updating of damaged slab from ambient vibration measurements, *Measurement* 46 (4) (2013) 1371–1378.
- [50] Y. An, H. Jo, B. Spencer Jr, J. Ou, A damage localization method based on the ‘jerk energy’, *Smart Mater. Struct.* 23 (2) (2013) 025020.
- [51] Y. Zhao, L.K. Foong, Predicting electrical power output of combined cycle power plants using a novel artificial neural network optimized by electrostatic discharge algorithm, *Measurement* 111405 (2022).
- [52] F. Marini, B. Walczak, Particle swarm optimization (PSO), A Tutorial, *Chemometrics and Intelligent Laboratory Systems* 149 (2015) 153–165.
- [53] J. Xue, B. Shen, A novel swarm intelligence optimization approach: sparrow search algorithm, *Systems Sci. Control Eng.* 8 (1) (2020) 22–34.
- [54] C. Szegedy, W. Liu, Y. Jia, P. Sermanet, S. Reed, D. Anguelov, D. Erhan, V. Vanhoucke, A. Rabinovich, Going deeper with convolutions, in: Proceedings of the IEEE Conference on Computer Vision and Pattern Recognition, 2015, pp. 1–9.
- [55] Z. Jia, Z. Liu, Y. Cai, A novel fault diagnosis method for aircraft actuator based on ensemble model, *Measurement* 176 (2021) 109235.